

# ULRR

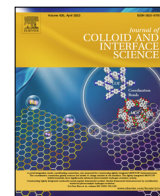
## Single core and multicore aggregates from a polymer mixture: A dissipative particle dynamics study

Item Type	Article
Authors	Javan Nikkhah, Sousa;Sammalkorpi, Maria
Citation	Journal of Colloid and Interface Science, 2023 635, pp. 231–241
Publisher	Elsevier
Download date	2026-06-16 18:34:39
Item License	<a href="https://creativecommons.org/licenses/by-nc-sa/4.0/">https://creativecommons.org/licenses/by-nc-sa/4.0/</a>
Link to Item	<a href="https://doi.org/10.34961/researchrepository-ul.23925351">https://doi.org/10.34961/researchrepository-ul.23925351</a>



Contents lists available at ScienceDirect

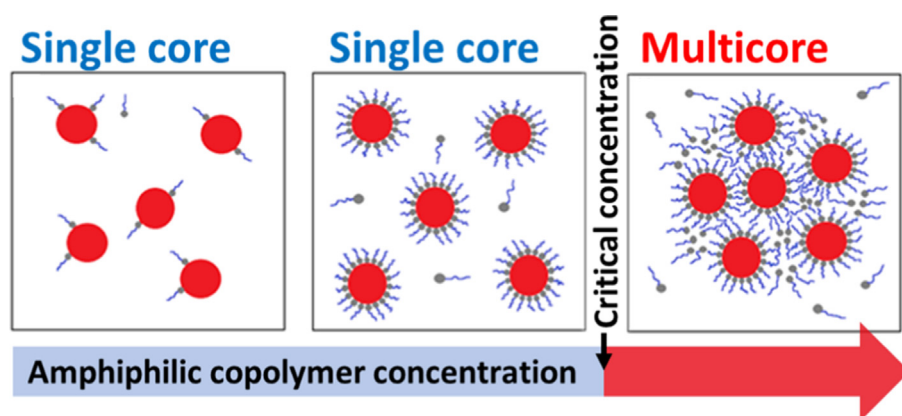
## Journal of Colloid and Interface Science

journal homepage: [www.elsevier.com/locate/jcis](http://www.elsevier.com/locate/jcis)

## Single core and multicore aggregates from a polymer mixture: A dissipative particle dynamics study

Sousa Javan Nikkhah<sup>a,b,c,\*</sup>, Maria Sammalkorpi<sup>a,e,f,\*</sup><sup>a</sup> Department of Chemistry and Materials Science, School of Chemical Engineering, Aalto University, P.O. Box 16100, FI-00076 Aalto, Finland<sup>b</sup> Department of Physics, Bernal Institute, University of Limerick, V94 T9PX Limerick, Ireland<sup>c</sup> Department of Chemical Sciences, Bernal Institute, University of Limerick, V94 T9PX Limerick, Ireland<sup>d</sup> Department of Bioproducts and Biosystems, School of Chemical Engineering, Aalto University, P.O. Box 16100, FI-00076 Aalto, Finland<sup>f</sup> Academy of Finland Center of Excellence in Life-Inspired Hybrid Materials (LIBER), Aalto University, P.O. Box 16100, FI-00076 Aalto, Finland

## GRAPHICAL ABSTRACT



## ARTICLE INFO

## Article history:

Received 18 August 2022

Revised 4 December 2022

Accepted 20 December 2022

Available online 23 December 2022

## Keywords:

Multicore aggregate

Single core–double shell aggregate

Polymeric aggregate

Structural transition

Coarse-grained simulations

Dissipative particle dynamics

## ABSTRACT

**Hypothesis:** Multicore block copolymer aggregates correspond to self-assembly such that the polymer system spontaneously phase separates to multiple, droplet-like cores differing in the composition from the polymer surroundings. Such multiple core aggregates are highly useful capsules for different applications, e.g., drug transport, catalysis, controlled solvation, and chemical reactions platforms. We postulate that polymer system composition provides a direct means for designing polymer systems that self-assemble to such morphologies and controlling the assembly response.

**Simulations:** Using dissipative particle dynamics (DPD) simulations, we examine the self-assembly of a mixture of highly and weakly solvophobic homopolymers and an amphiphilic block copolymer in the presence of solvent. We map the multicore vs single core (core–shell particles) assembly response and aggregate structure in terms of block copolymer concentration, polymer component ratios, and chain length of the weakly solvophobic homopolymer.

**Findings:** For fixed components and polymer chemistries, the amount of block copolymer is the key to controlling single core vs multicore aggregation. We find a polymer system dependent critical copolymer concentration for the multicore aggregation and that a minimum level of incompatibility between the

\* Corresponding authors.

E-mail addresses: [sousa.javannikkhah@ul.ie](mailto:sousa.javannikkhah@ul.ie) (S. Javan Nikkhah), [maria.sammalkorpi@aalto.fi](mailto:maria.sammalkorpi@aalto.fi) (M. Sammalkorpi).

solvent and the weakly solvophobic component is required for multicore assembly. We discuss the implications for polymer system design for multicore assemblies. In summary, the study presents guidelines to produce multicore aggregates and to tune the assembly from multicore aggregation to single core core-shell particles.

© 2022 The Authors. Published by Elsevier Inc. This is an open access article under the CC BY license (<http://creativecommons.org/licenses/by/4.0/>).

## 1. Introduction

Block copolymers self-assemble to various morphologies spontaneously [1–6]. The assembly is driven by demixing (or micro-phase separation) of the chemically dissimilar polymer segments into different domains [6–8]. In recent years, complex and fascinating supramolecular structures of block copolymers [9,10] such as micelles [11,12], films [13,14], tubules [15], and vesicles [16,17] have been produced by self-assembly. The assembly is driven by a combination of entropy and enthalpy [18–21]. Concentration, degree of polymerization, and miscibility of the components are the key parameters determining the final assembled morphology [21].

A particularly interesting type of self-assembling phase is the formation of multicore micelles. In macroscopic assembly, this corresponds to the droplet phase [22,23]. In both multicore micelles and the droplet phase, isolated domains of one polymer composition are surrounded by a corona phase with a differing composition. This leads to assemblies with several cores, see e.g. Refs. [24–29]. Multicore assemblies have attracted attention not only for academic reasons but also for their potential use in water purification, catalysis, pharmacology, electronics, and oil recovery [20,30–37].

Both experimental and theoretical research works have reported multicore micelles as one of their obtained results. Multicore micelles were formed by Duxin et al. [28] in cadmium sulfide (CdS) quantum dots (QDs) formation within poly(ethylene oxide)-*block*-polystyrene-*block*-poly(acrylic acid) (PEO-*b*-PS-*b*-PAA) triblock copolymer. Iatridi et al. [27] explored a novel multisegmented, multiarm star-shaped terpolymer bearing PS hydrophobic arms and P2VP-*b*-PAA diblock copolymer amphoteric arms in aqueous media leading to multicore large compound micelles. In another research work, Ueda et al. [26] observed a single core to multicore transition in amphiphilic alternating copolymer samples of sodium maleate and dodecyl vinyl ether via changing molecular weight. Liu et al. [38] studied the self-assembly of an amphiphilic hyperbranched homopolymer with alternating hydrophobic disulfide and hydrophilic polyphosphate segments resulting in multicore/shell structure micelles with a narrow size distribution. The multicore morphology, stability in aqueous solution, and responsivity to reductive environment, can make multicore assemblies an attractive platform for sequential drug-delivery e.g. in cancer therapy. Multicore micelles of iron oxide nanoparticles- oligomeric sodium undecylenate were produced by Naous et al. [39], reporting that the micelles displayed multiple mechanisms in retention of aromatic amines, e.g., dispersion, hydrogen bonding, polar, and ionic for solute solubilization. The high density of the micelles and the variety of interactions provided by this sorbent made the multicore micelles highly efficient for extracting aromatic amines in a broad polarity range from textiles, urine, and wastewater.

Computational studies have frequently contributed to understanding the relationship between experimental parameters and aggregation behaviour [40–43]. However, purely theoretical and computational approaches are well-established tools to explore also the collapse dynamics, phase separation, and the self-assembly in polymer solutions, see e.g. Refs. [44–49]. For example,

Wang et al. [25] used self-consistent field theory based calculations to discover complex multicore aggregates, such as the double-stranded superhelix, in a solution-state self-assembly system composed of linear ABC terpolymers consisting of a solvophilic block and two mutually incompatible solvophobic end blocks. Using self-consistent field theory based calculations, Guo et al. [50] could observe wormlike multicore micelles for  $\pi$ -shaped ABC block copolymers with a hydrophilic backbone block A and hydrophobic graft blocks B and C. The findings showed how the distance of the two graft blocks of the  $\pi$ -shaped block copolymers controls the morphology of wormlike multicore micelle. Chen et al. [29] identified multicore colloidal particles formed by self-assembling a three-arm star-shaped polymer using dissipative particle dynamics (DPD) simulations.

Although these studies demonstrate several interesting examples of realizations for stable, self-assembling block copolymer multicompartment and multicore aggregates, the synthesis methods are hard to implement. To fully utilize and benefit from the technological potential of the heterogeneous, compartmentalized molecular environment of the multicore and multicompartment aggregates, more economical and straightforward approaches to form multicore and multicompartment assemblies are needed. In our previous work [49], we reported multicore aggregation in a simple, three-component polymeric system based on DPD simulations. The focus polymer system composed of a mixture of highly and weakly solvophobic homopolymers and an amphiphilic block copolymer in a solvent medium. We extracted guidelines for the necessary solvophobicity differences in the polymer mixture components for spontaneous multicore assembly. Here, we provide a systematic characterization of the interdependencies of a simple three component linear copolymer system to self-assemble into multicore assemblies of several co-existing length scales vs traditional polymer core-shell micelles. The findings center on generalizations of assembly dependence, in particular necessity for a critical amount of copolymer, interconnected with the miscibility difference of the component species, as means to induce and control the dual length scale assembly. The findings suggest possible transition mechanisms and morphological transition variables to aid design of polymer self-assembly systems.

## 2. Methods

Dissipative particle dynamics (DPD) simulations [51–53] were used to examine the polymer system. DPD is a coarse-grained bead-based simulation method that can be used to describe at mesoscale complex liquids. The use of soft potentials and capturing hydrodynamics make the approach useful for examining the assembly and dynamics of soft matter in the liquid phase. While the approach captures assembly and morphology changes very efficiently, retaining chemical mean characteristics of the modelled molecular region, the coarse-graining loses strongly localized and microscopic level effects, such as charge-charge pairing effects or hydrogen bonding.

The total force  $\vec{F}_i$  acting on particle  $i$  is composed of pairwise conservative force  $\vec{F}_{ij}^C$ , friction force  $\vec{F}_{ij}^D$ , stochastic force  $\vec{F}_{ij}^R$ , and

a harmonic spring force  $\vec{F}_{ij}^S$  between the polymer beads such that

$$\vec{F}_i = \sum_{i \neq j} \left( \vec{F}_{ij}^C + \vec{F}_{ij}^D + \vec{F}_{ij}^R + \vec{F}_{ij}^S \right) \quad (1)$$

In this,  $\vec{F}_{ij}^C = a_{ij} \omega^C(r_{ij}) \vec{e}_{ij}$ , the hydrodynamic drag is captured by  $\vec{F}_{ij}^D = -\gamma \omega^D(r_{ij}) (\vec{v}_{ij} \cdot \vec{e}_{ij}) \vec{e}_{ij}$  and  $\vec{F}_{ij}^R = \sigma \omega^R(r_{ij}) \theta_{ij} \vec{r}_{ij}$  corresponds to thermal fluctuations and has Gaussian distribution. A harmonic spring force  $\vec{F}_{ij}^S = k \vec{r}_{ij}$ , with spring force constant  $k = 4$  in DPD reduced units, is set between neighboring polymer beads to keep the polymer beads connected [19,53,54]. The total force  $\vec{F}_i$  (Eq. (1)) is summed over all particles  $i \neq j$  for the conservative, friction, and stochastic forces at separations less than the cutoff radius  $R_C$ . The spring force acts only between consecutive beads in a polymer chain.

Additionally,  $\vec{r}_{ij} = \vec{r}_i - \vec{r}_j$ ,  $r_{ij} = |\vec{r}_{ij}|$ , and  $\vec{e}_{ij} = \frac{\vec{r}_{ij}}{r_{ij}}$ , with  $\vec{r}_i$  and  $\vec{r}_j$  being the position vectors of particle  $i$  and  $j$ , respectively. The relative velocity  $\vec{v}_{ij} = \vec{v}_i - \vec{v}_j$ , where  $\vec{v}_i$  and  $\vec{v}_j$  capture the velocities of particle  $i$  and  $j$ , respectively. The interaction parameter  $a_{ij}$  captures repulsion between the particles,  $\gamma = 4.5$  is the friction coefficient, and  $\sigma = 3$  the noise amplitude governing the intensity of the stochastic force. The conservative, dissipative, and random forces each include their own weight function called  $\omega^C$ ,  $\omega^D$ , and  $\omega^R$ , respectively. For the conservative force,  $\omega^C(r_{ij}) = 1 - \frac{r_{ij}}{R_C}$  for  $r_{ij} < R_C$  and  $\omega^C(r_{ij}) = 0$  for  $r_{ij} \geq R_C$ . The two weight functions  $\omega^D(r_{ij})$  and the  $\omega^R(r_{ij})$  can be chosen arbitrarily but their relation is  $\omega^D = [\omega^R(r_{ij})]^2$  [52]. A simple form of  $\omega^D$  and  $\omega^R$  was chosen following Groot and Warren [53] with  $\omega^D(r_{ij}) = [\omega^R(r_{ij})]^2 = \left(1 - \frac{r_{ij}}{R_C}\right)^2$  for  $r_{ij} < R_C$  and  $\omega^D(r_{ij}) = [\omega^R(r_{ij})]^2 = 0$  for  $r_{ij} \geq R_C$ . The amplitudes follow  $\sigma^2 = 2\gamma k_B T$  based on fluctuation–dissipation theorem, so that the dissipative force and random force together act as a thermostat.  $\theta_{ij}(t)$  is a Gaussian random variable with zero-mean and unit variance [54]. DPD simulations keep the particle number, volume, and temperature constant and take place in the NVT ensemble.

A modified velocity-Verlet algorithm is used to integrate the equations of motion with a time step  $\Delta t = 0.05 t$  and weighting factor  $\lambda = 0.65$ . Unit normalization follows standard DPD reduced units such that the cutoff radius  $R_C$ , the bead mass  $m$ , and  $k_B T$ , where  $k_B$  is the Boltzmann constant and  $T$  the temperature, are used as the distance, mass, and energy units. This leads to  $R_C = m = k_B T = 1$  and the time unit  $\tau = (mr^2 / k_B T)^{1/2} = 1$ . The particle number density in the system is set to  $\rho = 3$ . With this choice, the relationship between the DPD  $a_{ij}$  interaction parameter and Flory-Huggins mixing parameter  $\chi_{ij}$  is

$$a_{ij} - a_{ii} \approx 3.27 \chi_{ij} \quad (2)$$

A value of  $a_{ii} = 25$  is set for the same type of DPD particles. A summary of the DPD reduced units and their conversions, as well as those of the model parameters are presented in the Supporting Material in Table S1.

## 2.1. Model construction details

The examined system consists of an amphiphilic diblock copolymer and two linear homopolymers, one weakly and the other strongly solvophobic, mixed in a solvent. All examined chains correspond to oligomeric chain length range. To simplify the modelling system, the blocks of the copolymer are considered

identical in their interactions to the two homopolymer species. This leads to three different types of DPD beads in the system A, S, and W. The two former compose the two homopolymers  $A_n$  and  $S_m$  and the diblock copolymers  $A_k S_l$ , where the subindexes refer to the number of beads in the chain, see Fig. 1. The solvent is described by beads W. All beads have the same size and mass  $m = 1$ . Table 1 summarizes the examined concentrations, chain lengths and chain length variable indices used in the work. The concentrations were chosen to be likely to result in finite size aggregates, and to be typical aqueous solution concentrations of such polymer solutions. The concentration of species  $i$ ,  $C_i$ , is calculated as the species fraction, i.e. the number of beads of species  $i$  divided by the total number of DPD beads in the system. As the DPD beads all have equal volume and mass, this fraction leads to weight and volume concentration percentages. The copolymer concentration  $C_{A_1 S_6}$  and the weakly hydrophobic homopolymer chain length are the two main parameters studied in this research as morphology controlling factors.

The interaction parameters are identical to those in our previous work [49]:

$$a_{ij} = \begin{Bmatrix} A & S & W \\ A & 25 & 72 & 115 \\ S & 72 & 25 & 30 \\ W & 115 & 30 & 25 \end{Bmatrix}$$

For polymer solutions, the transition to a poor solvent happens at  $\chi_{ij} = 0.5$ . Mixing parameter values above that critical value correspond to poor solvent. For theta condition, this leads to DPD interaction between polymer and solvent  $a_{ij} = 26.63$ , following Eq. (2). As in our model, the S-W interaction parameter  $a_{SW} = 30$  exceeds this, some phase separation can be expected. On the other hand, A and S are chosen to be strongly immiscible with  $a_{AS} = 115$ . This leads to a system that it is composed of solvophobic homopolymers A, amphiphilic copolymers composed of A and S blocks, and a slightly solvophilic homopolymer S.

The simulations were carried out using the LAMMPS (Large-scale Atomic/Molecular Massively Parallel Simulator) package [55,56] in a cubic simulation box  $40 R_C \times 40 R_C \times 40 R_C$  in size and periodic in all three dimensions. The simulation times were between  $5 \times 10^5$  and  $5 \times 10^6$  steps. Configurations and corresponding data were saved as frames at 2000 DPD steps intervals. Unless otherwise said, all presented data results from averaging over the last 20 saved frames. The analyzed data period corresponds to equilibrated systems; equilibration was evaluated against time evolution of aggregate structure (data provided in Supplementary Material Figure S1). Standard deviation is used as error estimate. Presented snapshots correspond to the final simulation configurations.

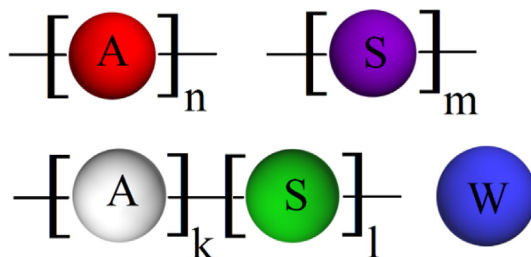


**Fig. 1.** Generic coarse-grained model for the system composed of two linear homopolymers, an amphiphilic diblock copolymer, and solvent described as  $A_n$ ,  $S_m$ ,  $A_k S_l$ , and W. The subindexes refer to the number of beads in each homopolymer or copolymer. The bead color coding is used for all figures.

**Table 1**

Component concentrations and compositions. The concentration percentage of species  $i$  is calculated based on (Number of beads of species  $i$ ):(Total number of beads).

	$A_n$	$S_m$	$A_1S_6$
Concentration (%)	4.0	3.2	$C_{A_1S_6}$
Chain length (beads)	19	$m$	$\frac{6}{1}$

### 3. Results and discussion

#### 3.1. Block copolymer concentration

First, the effect of block copolymer concentration,  $C_{A_kS_l}$  on the self-assembled morphology was examined. The other system parameters were kept constant:  $A_{19}$  and  $S_6$  concentrations were  $C_{A_{19}} = 4.0\%$  and  $C_{S_6} = 3.2\%$ , respectively and the block copolymer was  $\frac{1}{k} = \frac{6}{1}$ , that is,  $A_1S_6$ . Its concentration was varied as  $C_{A_kS_l} = 2.0\%$ ,  $3.0\%$ ,  $5.0\%$ ,  $13.0\%$ ,  $20.0\%$ ,  $25.0\%$ , and  $30.0\%$ .

Fig. 2 shows the final morphologies as a function of  $A_1S_6$  concentration. With increasing concentration, the system undergoes a transition from well-defined, single core, soluble core-shell assemblies (Fig. 2a and 2b) to associating morphologies with internal, multicore structures. The intermediate states correspond to the core-shell assemblies showing increasing adhesion, which translates to first chain-like assembly and, at larger adhesion, more compact packing. We note that the exact assembly morphology is subject to simulation system size, i.e. when the assemblies start aggregating and for example, the elongated chain (Fig. 2d) or the multicore particle (Fig. 2e) formed in the simulations could actually correspond to macroscopic aggregation, given a larger simulation system. Similarly, the system spanning assemblies (Fig. 2f-h) are subject to system periodicity in their morphology. Hence, in our analysis and discussing the results, we focus on changes in the internal structure and adhesion mechanisms.

The cross-sections of the single core aggregates formed at 2 % and 3 % block copolymer concentration show a well-defined

core-double shell structure. The highly solvophobic components form spherical core composed of the  $A_{19}$  homopolymer and the more solvophobic block of the copolymer. The outer shell of the assembly is by the weakly solvophobic block of the copolymer and the  $S_6$  homopolymer. Correspondingly, in the multicore assembly, small cores of the highly solvophobic components are surrounded by the weakly solvophobic blocks and homopolymer.

Increasing the concentration from 2.0 % to 5.0 % reveals the difference in assembly process between the single core and the multicore assemblies, see Fig. 3. For both type of assemblies, first cores composed of the highly solvophobic particles formed (Fig. 3a and 3f). These evolved into core-double shell assemblies in the growth process (Fig. 3b and 3g). Coalescence of these small core-double shell aggregates lead to formation of the final core-double shell aggregates in the single core assembly (Fig. 3c-e). Coalescence of the aggregates decreases their solvent accessible surface which aids the 2.0 % concentration of block copolymer chains in the system in coating the highly solvophobic core surface. The assembly formation is guided by the low copolymer concentration – the system does not have enough copolymer chains to stabilize small aggregates. On the other hand, at 5.0 % block copolymer concentration, the copolymer concentration is high enough to stabilize the small single core-double shell aggregates. Due to the weakly hydrophobic character of the  $S_6$  polymer and the corresponding block of the copolymer  $A_1S_6$ , the small single core-double shell aggregates gather together to form multicore aggregates (Fig. 3h-j). Consequently, it can be concluded that single core-double shell aggregates form via a combination of initial nucleation, growth, and aggregate coalescence, while the multicore aggregate structure arises from two of these sequences superposed, one corresponding to formation of the small initial aggregates and their growth and coalescence and another, slower one, to the assembly of the formed aggregates and corresponding response.

Analysis of the aggregate structures reveals that increasing the block copolymer concentration leads to the number of highly solvophobic cores increasing (see Fig. 4). Furthermore, the number of cores  $N_c$  versus copolymer concentration  $C_{A_1S_6}$  exhibits a differ-

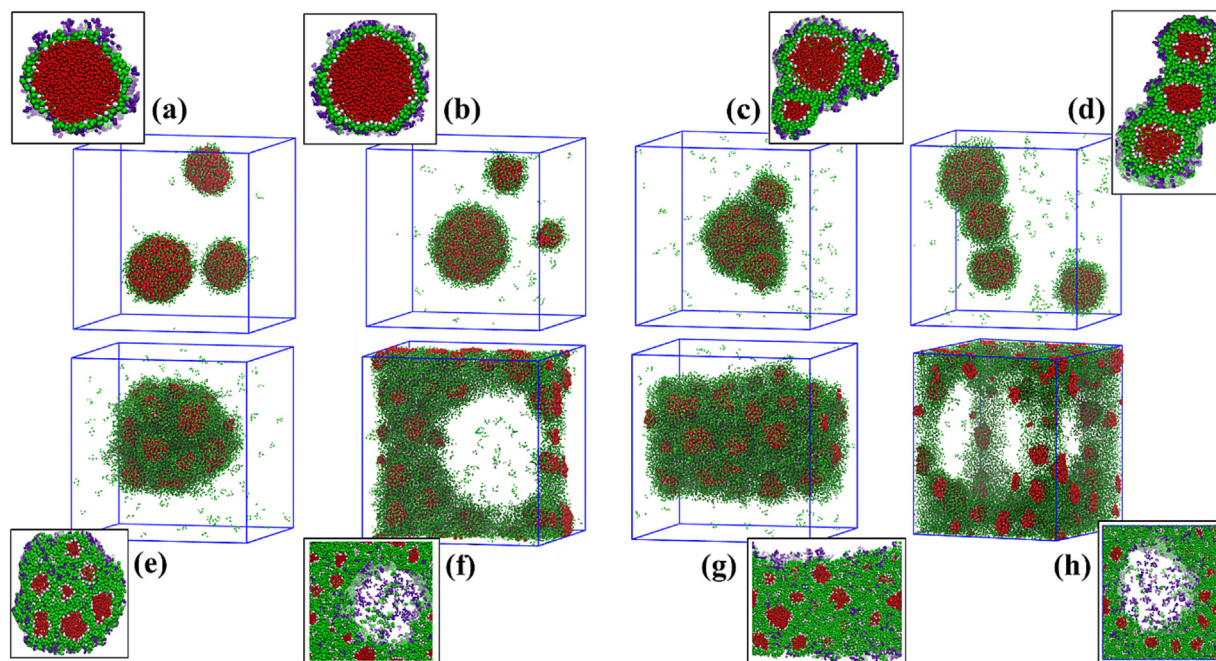


**Fig. 2.** Effect of increasing copolymer  $A_1S_6$  concentration on the assembly configurations. The examined systems correspond to keeping  $A_{19}$  and  $S_6$  concentrations constant at  $C_{A_{19}} = 4.0\%$  and  $C_{S_6} = 3.2\%$  while varying the  $A_1S_6$  block copolymer concentration in solvent. The block copolymer concentration increases from (a) to (h) with (a) 2.0 %, (b) 3.0 %, (c) 4.0 %, (d) 5.0 %, (e) 13.0 %, (f) 20.0 %, (g) 25.0 %, and (h) 30.0 %. Solvent beads are omitted for clarity. The coloring of particles follows Fig. 1.

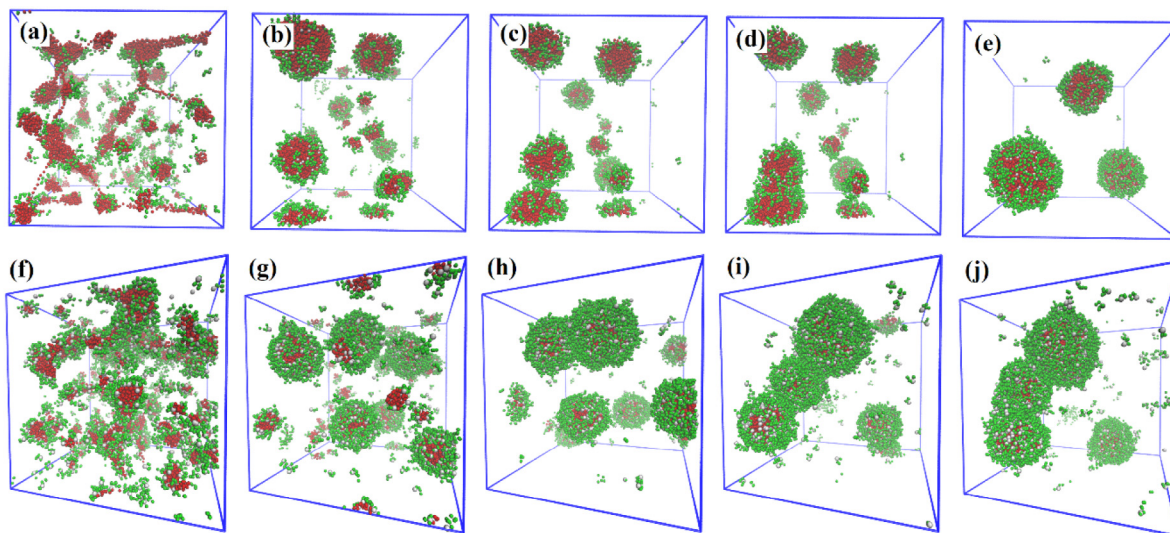


**Fig. 3.** Assembly process leading to single core (top row) and multicore assemblies (bottom row). The snapshots correspond to time evolution of the system from left to right for (a)–(e) 2 % and (f)–(j) 5 % of copolymer  $A_1S_6$ . The snapshots correspond to (a)  $3.0 \times 10^4$ , (b)  $3.0 \times 10^3$ , (c)  $1.2 \times 10^4$ , (d)  $1.8 \times 10^4$ , (e)  $5.0 \times 10^5$ , (f)  $3.0 \times 10^6$ , (g)  $4.0 \times 10^3$ , (h)  $2.5 \times 10^4$ , (i)  $4.0 \times 10^5$ , and (j)  $5.5 \times 10^5$  simulation timesteps. The examined systems correspond to keeping  $A_{19}$  and  $S_6$  concentrations constant at  $C_{A_{19}} = 4.0\%$  and  $C_{S_6} = 3.2\%$ . Solvent and  $S_6$  beads are omitted for clarity. The coloring of particles follows Fig. 1.

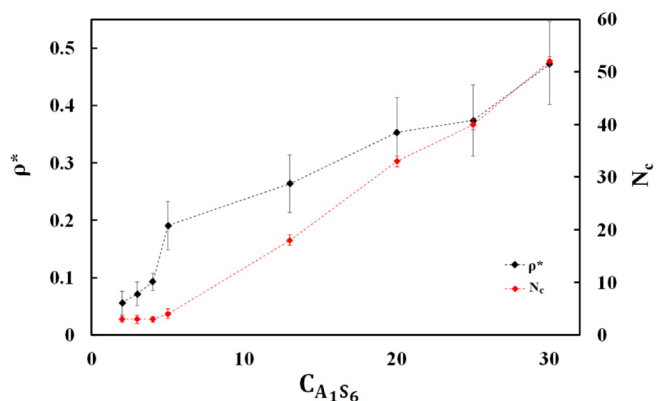


**Fig. 4.**  $\rho^*$  and number of the solvophobic cores  $N_c$  versus copolymer  $A_1S_6$  concentration  $C_{A_1S_6}$ . The examined systems correspond to keeping  $A_{19}$  and  $S_6$  concentrations constant at  $C_{A_{19}} = 4.0\%$  and  $C_{S_6} = 3.2\%$ .

ent slope for the single core and multicore regions. The slope change occurring between 4.0 % and 5.0 % copolymer concentration can be taken as the indicator for the transition from single core to multicore assembly.

Multicore aggregates are clearly present in copolymer concentration higher than 4 %. The significance of the finding is that, in this type of system, to have multicore aggregation, a minimum concentration of the stabilizing interfacial polymer, here the block copolymer, is essential. We call this limit the critical multicore aggregate concentration (CMAC). This is presented in a schematic diagram in Fig. 5. In copolymer concentrations lower than CMAC, the amount of block copolymer chains is insufficient to coat the surface of the cores completely which leads to regions of high surface tension at the solvent exposed highly solvophobic surface (see Fig. 5a). This drives the highly solvophobic cores to merge into larger cores (see Fig. 3a–e) to reduce the overall surface area. Core coalescence and growth occur until the copolymer concentration is sufficient to stabilize the amount of solvophobic surface in the system.

Adding more block copolymer to the system decreases interfacial surface tension between the highly solvophobic cores and the

solvent already at smaller core sizes. Additionally, as the resulting coating is weakly solvophobic, the stabilized small cores assemble to multicore aggregates. The observed CMAC corresponds to the lowest copolymer concentration sufficient to coat all highly solvophobic core surface such that the small aggregates are stable (see Fig. 5b). This makes CMAC a measure for the efficiency of the block copolymer to lower interfacial surface tension between the highly solvophobic domains and the solvent.

To analyze this, let us define  $\rho^* = N_{S-coat}/N_{A-core}$  to measure how effectively the highly solvophobic core surface area is coated. In this  $N_{S-coat}$  is the number of block copolymer beads  $S$  at the core surface and  $N_{A-core}$  is the number of highly hydrophobic  $A$  beads forming the core. A cut-off distance of 0.9 is used in defining neighboring DPD beads. For determining hydrophobic core surface particles  $N_{A-core}$ , either a  $W$  or  $S$  bead need to be within cut-off from an  $A$  bead in the analysis.  $N_{S-coat}$  is counted as the  $S$  beads neighboring the core surface beads. Fig. 4 presents the average  $\rho^*$  calculated over all cores in each system. A sharp increase in  $\rho^*$  versus  $C_{A_1S_6}$  curve, between 4 % and 5 % is detected, corresponding to the slope change in the  $N_c$  versus  $C_{A_1S_6}$  curve. Here, we observe a CMAC of around 4 % copolymer for this specific system. We emphasize that the significance of the finding is that this limit exists: the absolute number is clearly dependent on the examined system, for example, concentration of the other components, the level of solvophobicity of the polymers (chemistry of the components), chain lengths, and temperature.

### 3.2. Concentration ratios

Next the concentration ratios  $CR_{AA}$  and  $CR_{AS}$  were varied. Here,  $CR_{AA}$  is defined as  $(A_{19} \text{ chains}):(A_1S_6 \text{ chains})$  and  $CR_{AS}$  as  $(A_1S_6 \text{ chains}):(S_6 \text{ chains})$ , i.e. both by the ratio of the number counts of the respective chains. The total solid concentration was kept constant at 20.2 %. The solvent concentration in all studied systems was 79.8 % corresponding to 153,312 solvent beads in the box  $40 R_c \times 40 R_c \times 40 R_c$  in size.

Fig. 6 shows that increasing  $CR_{AA}$  induced a transition from multicore to single core structure (see the cross sections in Fig. 6). Increasing the number of  $A_{19}$  chains while decreasing the number of  $A_1S_6$  chains resulted in the block copolymers no longer

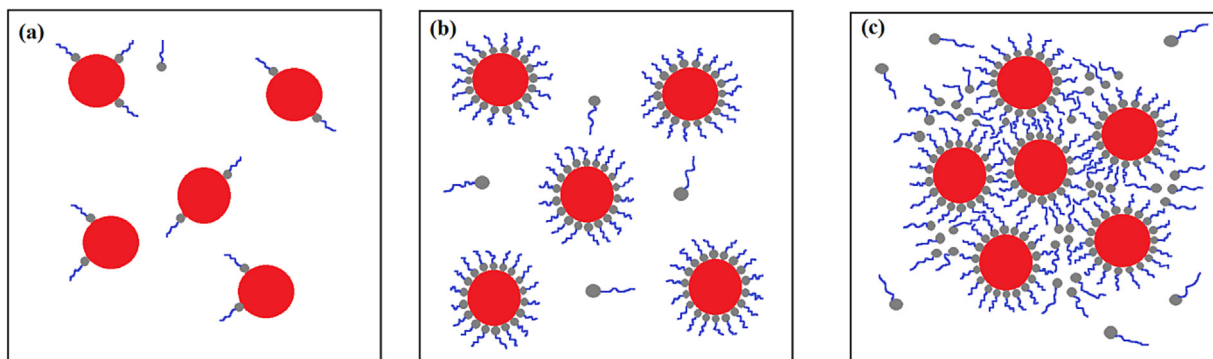


**Fig. 5.** Schematic cartoon of the effect of block copolymer concentration on the morphology of the aggregate. In (a) and (b), copolymer concentrations are less than CMAC, while (c) corresponds to the concentration exceeding CMAC. The red regions depict the highly solvophobic cores, while the copolymer blocks are shown in gray (highly solvophobic) and blue (weakly solvophobic), respectively. (For interpretation of the references to color in this figure legend, the reader is referred to the web version of this article.)

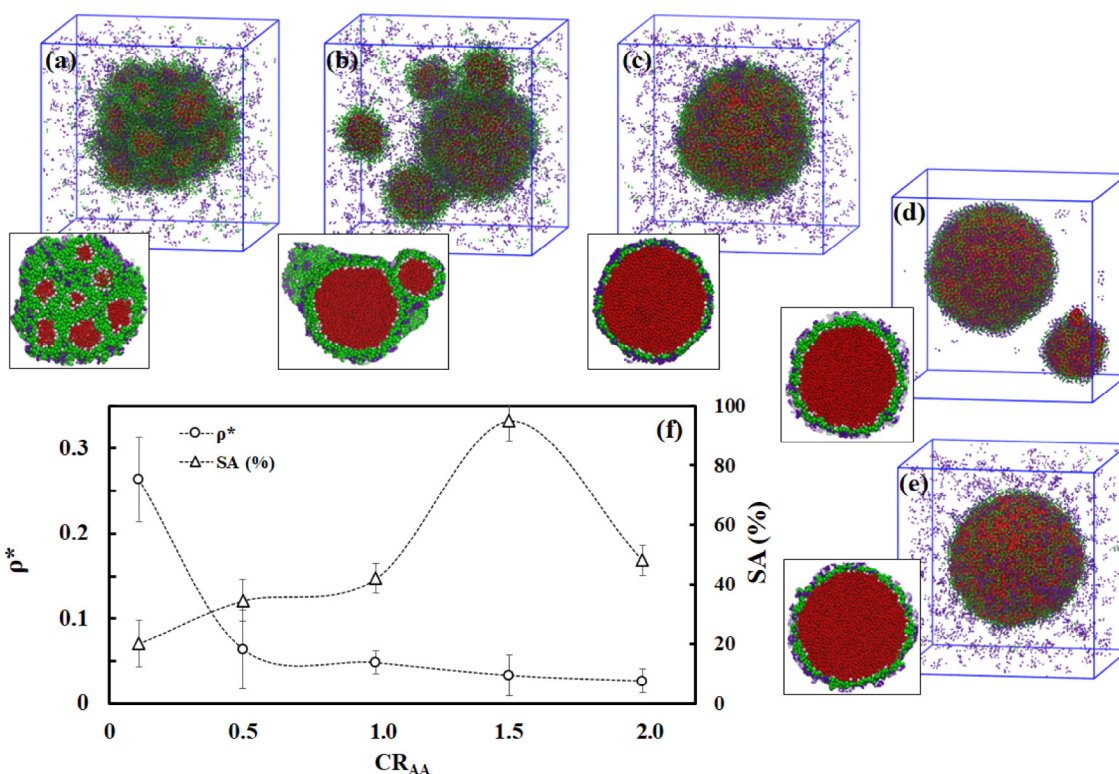


**Fig. 6.** Effect of varying the concentration ratio  $CR_{AA} = (A_{19} \text{ chains}) : (A_1S_6 \text{ chains})$ . The system studied contains  $A_{19}$  and  $A_1S_6$  in varying concentration ratio  $CR_{AA}$  and  $S_6$  in concentration  $C_{S_6} = 3.2\%$  in solvent. The snapshots correspond to  $CR_{AA}$  (a) 0.1, (b) 0.5, (c) 1.0, (d) 1.5, and (e) 2.0. (f)  $\rho^*$  and the  $S_6$  homopolymer adsorption percentage SA versus  $CR_{AA}$ . Total solid concentration is kept constant at 20.2%. Solvent beads are omitted for clarity. The coloring of particles follows Fig. 1. Three statistically independent simulation runs for each system were performed.

being sufficient to form a shell around the cores. As before, to reduce interfacial surface tension between the highly solvophobic core surfaces and solvent, the cores fused. Correspondingly, the  $\rho^*$  curve showed a decrease in adsorbed  $A_1S_6$  on the highly solvophobic cores.

Fig. 6 also shows by the adsorbed  $S_6$  (SA%) versus  $CR_{AA}$  data that an increase of the number of  $A_{19}$  chains (and the corresponding decrease in the number of block copolymer chains) lead to  $S_6$  chain adsorption to the aggregate first increasing and then with an even larger  $CR_{AA}$ , decreasing. This is because the highly hydrophobic cores first increased in size and simultaneously the  $A_1S_6$  concentration decreased as  $CR_{AA}$  increased. This led to the available contact area between the highly solvophobic cores and the  $A_1S_6$  chains

increasing, which promoted adsorption of the  $A_1S_6$  chains and resulted in less steric hindrance. Consequently,  $A_1S_6$  chains can cover the highly solvophobic core better and more  $S_6$  chains adsorbed on the surface. However, when  $CR_{AA}$  increased further, the  $A_1S_6$  was no longer sufficient to coat the entire core surface. This resulted in more exposed surface for the cores, which repelled some of the  $S_6$  chains.

The effect of  $CR_{AS} = (A_1S_6 \text{ chains}) : (S_6 \text{ chains})$  variation in the range 0.5–6 is presented in Fig. 7a–e. The corresponding time evolution of the number of cores is presented in the Supporting Information, Figure S1. A decrease of  $CR_{AS}$  clearly pushes the assembly toward single core aggregate formation. However, a complete transition from the multicore assembly does not occur in the examined

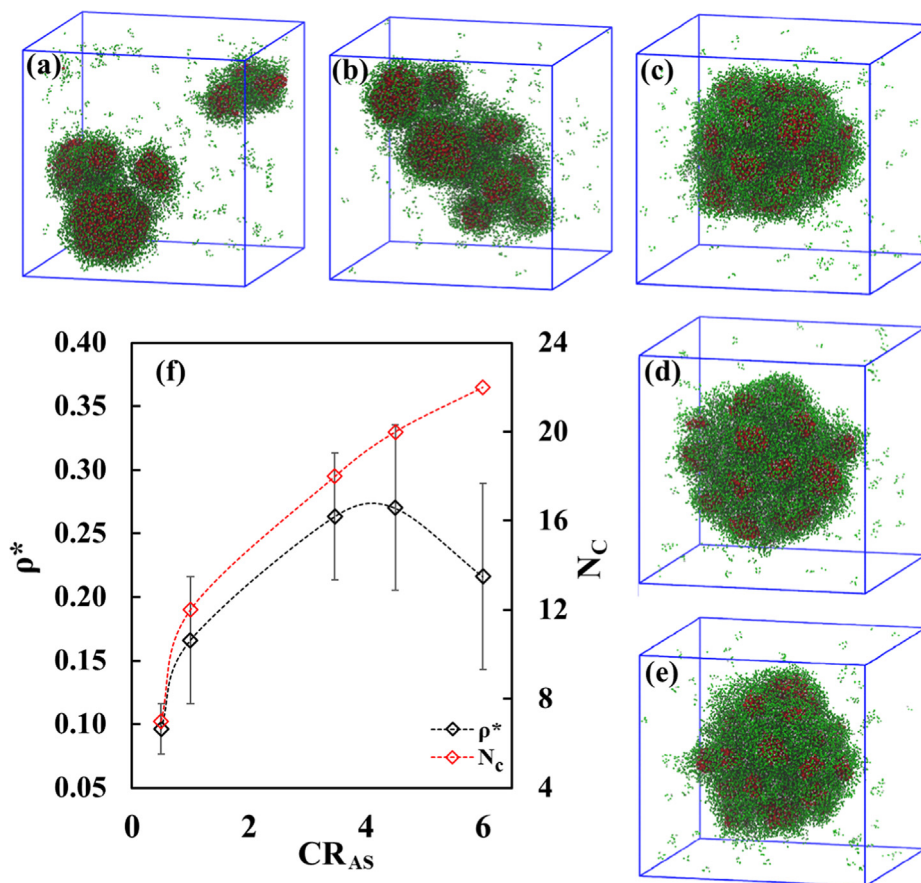


**Fig. 7.** Effect of varying the concentration ratio  $CR_{AS} = (A_1S_6 \text{ chains}) : (S_6 \text{ chains})$ . The system studied contains  $A_{19}$  in concentration 4.0 % and  $A_1S_6$  and  $S_6$  in varying concentration ratio  $CR_{AS}$  in solvent. The snapshots correspond to  $CR_{AS}$  (a) 0.5, (b) 1.0, (c) 3.5, (d) 4.5 and (e) 6.0. (f)  $\rho^*$  and core number count  $N_c$  curves versus  $CR_{AS}$ . Total solid concentration is kept constant at 20.2 %. Solvent and  $S_6$  beads are omitted for clarity. The coloring of particles follows Fig. 1. Snapshots showing more details and the cross-section cuts of the aggregates are presented in the Supporting Information, Figures S2 and S3, respectively.

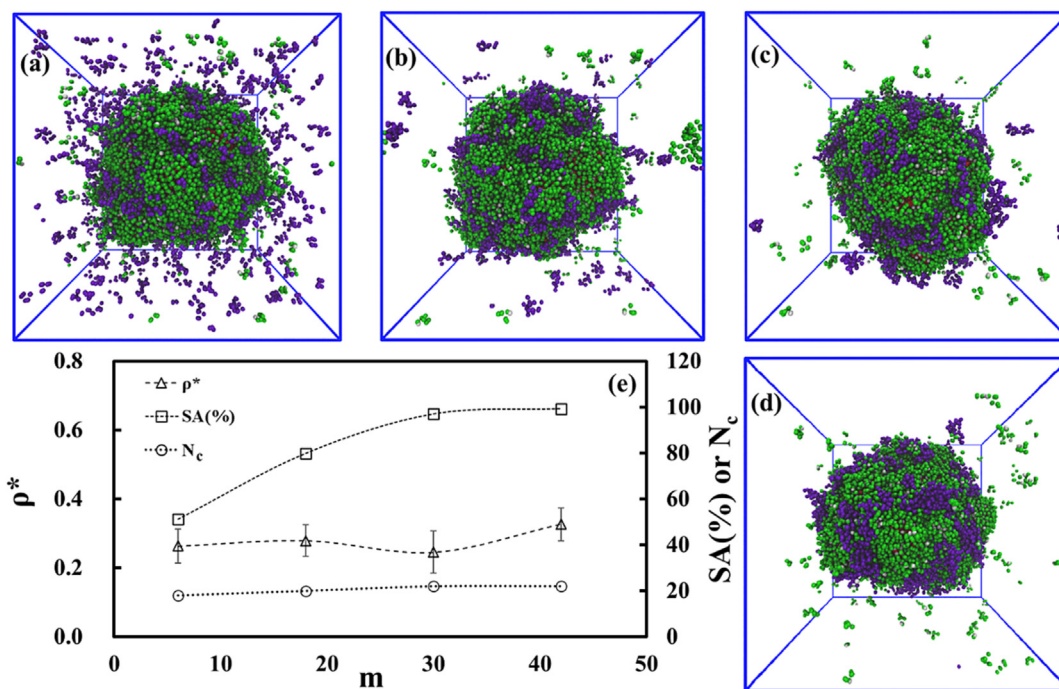


**Fig. 8.** Final snapshots corresponding to a polymer system with  $A_{19}$  (4.0 %),  $A_1S_6$  (13.0 %) and  $S_m$  (3.2 %), with varying  $S_m$  chain length  $m$  in solvent. The snapshots correspond to a)  $m = 6$ , b)  $m = 18$ , c)  $m = 30$ , and d)  $m = 42$ . In e),  $\rho^*$ , SA and  $N_c$  curves versus  $m$  are plotted. Total solid concentration is kept constant at 20.2 %. Solvent beads are omitted for clarity. The cross-section visualizations of the aggregates are presented in the Supporting Material Figure S4.

range. However, an even smaller  $CR_{AS}$  can be expected to lead to single core formation, see discussion in Section 3.1. Furthermore, increasing  $CR_{AS}$  leads to an increase in the number of highly solvophobic cores in the examined system (Fig. 7f). The considerations presented before concerning aggregate fusion until block copolymer stabilization is sufficient to stabilize the assemblies are valid here as well.

Notably,  $\rho^*$  passes through a maximum with increasing  $CR_{AS}$ . The adsorbed  $S_6$  chains act as a binder for small aggregates and pack with the  $S_6$  blocks of the copolymer such that the copolymer block elongation decreases. This leads to less elastic deformation penalty in the conformations. An increasing copolymer concentration corresponds to the concentration of  $S_6$  decreasing in an effective coating of the solvophobic cores. This indicates that the copolymer and  $S_6$  can compensate each other in the coating formation.

### 3.3. Chain length variation of the weakly solvophobic homopolymer

The effect of the chain length on the overall aggregation of the homopolymer chains  $S_m$  is essential as this polymer species facilitates the agglomeration of the multicore assemblies. We varied  $m$  between 5 and 42 DPD beads while keeping the total solids concentration constant. Fig. 8 shows that increasing  $m$  decreased the concentration of  $S_m$  in solvent as the longer  $S_m$  chains were mainly adsorbed to the aggregate. Fig. 8f presents a quantification of this by the adsorbed  $S_6$  percentage (SA%) versus  $m$ . The data shows an increasing trend for the adsorption with increasing chain length, with the longer chain lengths leading to almost total adsorption of the  $S_m$ . Increasing the chain length lead additionally to a proportionally higher connectivity between the beads. This restricted the motions of the beads and promoted adsorption. On the other hand, increasing  $m$  decreased the chain solubility since polymer solubility decreases with an increasing degree of polymerization. Consequently, the chains preferred to diffuse inside the aggregate or to adsorb to the aggregates. This reduced their contact with solvent.

Increasing  $m$  did not change the multicore aggregate structure. To quantify this,  $\rho^*$  and  $N_c$  curves versus  $m$  are presented in Fig. 8e. The data shows no significant changes within the examined  $m$  range.

## 4. Conclusions

Recently, multicore or multicore–multicompartment assemblies have been produced successfully by various approaches such as self-assembly of triblock copolymers [28,57–60], amphiphilic alternating copolymers [26], linear ABCBA penta-block copolymers [61], and via triblock copolymer non-linear architectures such as star-shaped, miktoarm, and dendritic [27,62,63]. Despite all these studies demonstrating multicore and multicompartment micellar assembly, the polymer systems for which multicore or multicompartment assembly morphologies have been established remain relatively complex. Additionally, multicore assembly and control of the multicompartment assemblies remain open topics at the microscopic level.

Here, we presented a simple three component linear polymer system that self-assembles to multicore assemblies with two co-existing characteristic structural assembly length scales. In particular, the system corresponds to a cost-efficient and simple block-copolymer framework containing a strongly solvophobic homopolymer, a weakly solvophobic species and an amphiphilic block copolymer in a solvent medium. We found that the examined model system self-assembles into two main self-assembly structures: 1) single core and 2) multi core assemblies. The main

findings center around the systematic design and tuning of the assembly characteristics and emergence of the multiple length scales allowed by the system parameters. Specifically, we mapped on the selected model system the dependency of the assembly structure and the single core to multi core assembly transition on the copolymer concentration, component concentration ratios, and chain length of the weakly solvophobic homopolymer acting as binder in the multicore assembly.

At low block copolymer concentrations, single core assemblies formed while an increase in the block copolymer led to the assembly transitioning to multicore. The findings indicate that a minimum concentration of the block copolymer is essential to have multicore aggregates. We postulate that this leads to an effective critical multicore aggregate concentration (CMAC) for the examined system and its analogues. The results suggest that at copolymer concentrations lower than CMAC, the polymer system has less block copolymer chains than required for complete coating of the surface of the solvophobic cores. Thus, reducing the interfacial surface tension by the amphiphilic block copolymer remains incomplete. A further reduction in the overall aggregation free energy can be achieved by the highly solvophobic cores merging to form larger cores that have correspondingly a smaller total surface area to coat by the amphiphilic copolymers. Hence, CMAC corresponds to the concentration at which the surface tension reduction by the copolymer chains counters the free energy gain of the cores merging, leading to stabilization of the small cores. Given sufficient corona attraction (in this work, the weak solvophobicity of the  $S$  polymer component), the small aggregates may form multicore assemblies. It is worth noting that a highly solvophilic corona would lead to small, soluble core–shell particles, instead of the multicore assembly.

In line, the simulations also showed that a transition from multicore to single core structures can be achieved by increasing the number of highly solvophobic homopolymer chains while decreasing the number of copolymer chains such that the total solids concentration remained constant. Varying the number ratio of the block copolymer chains and the weakly solvophobic homopolymer chains again resulted in the system transitioning from multicore assembly to single core assembly at low block copolymer to weakly solvophobic homopolymer ratio. Both transitions can be understood in terms of the change resulting in an insufficient amount of block copolymers to form a shell around the cores.

A different mechanism of assembly change was observed when varying the weakly solvophobic homopolymer chain length. Increasing the length of the weakly solvophobic homopolymer led to decrease of its concentration in solvent as the longer chains are mainly adsorbed onto the aggregate shell. This is a direct consequence of the decrease in solubility by the increase of length. Additionally, as adsorption of more and longer chains onto the corona increase both the corona size and the extension of the corona polymers to the solvent phase, the corona becomes potentially more adhesive, promoting multicore assembly in comparison to core–shell particle formation. In total, the results lead to conclusion that an interplay between the interfacial surface tension driving for hydrophobic core growth, the availability of enough copolymer chains to stabilize the formed solvophobic cores, and a sufficient adhesion stickiness (here, the weak hydrophobicity) of the stabilizing corona are responsible for multicore aggregate formation and the stability of the assembly. We mapped the dependency of these for several system variables in a simple, generalizable three component polymer system.

Notably, multicore aggregates have significant advantages in comparison to regular core–shell micelles: the cores provide microenvironments differing from their surroundings, and for stimuli-responsive polymer system, parameters such as pH, salt concentration, temperature, electromagnetic field, light,

ultrasound, and enzymes, can be used for tuning [32–34,36,37,64,65]. This is interesting for high-precision solubilization and control of release, e.g. in sequential drug delivery type applications where the cores are loaded with multiple drug types released stepwise [66,67]. The multicore, confined microenvironment capsules can protect the carried species, for example, drugs or reactants. For drugs, this means enhanced prevention of enzymatic degradation, improved biodistribution, and decrease of drug uptake in unwanted tissues [66,67]. For catalysis and reactions platforms, a corresponding enhancement of reaction and product control is obtained [33,34].

The presented findings agree with previously reported findings on alkyl-ethoxylate and pluronics block copolymer systems dependency on amphiphilic component concentrations in particular assembly and assembly morphologies [68–71]. Systematic assembly studies besides the alkyl-ethoxylate and pluronics model systems remain rare but findings include e.g. amphiphile concentration based controlled melting of poly(butyl acrylate-*b*-acrylic acid) micelles [72] and directing assembly structure of sodium poly(isoprene-*b*-methacrylate) micelles [73]. At general level, amphiphiles and their concentration are well-known to control assembly morphologies in polymeric systems, for recent reviews see e.g. Refs. [74,75]. However, the responses have been demonstrated for individual polymer mixtures. Here, we mapped the dependency of system parameters for an easily generalizable polymer system and identify specific requirement of amphiphilic component for the dual length scale, multicore assembly. The significance of the current computational work is that the revealed trends and observed transitions can aid in designing polymer systems for controlled multicore assembly.

#### CRedit authorship contribution statement

**Sousa Javan Nikkhah:** Methodology, Investigation, Conceptualization, Software, Validation, Formal analysis, Data curation, Visualization, Writing – original draft, Writing – review & editing. **Maria Sammalkorpi:** Supervision, Conceptualization, Resources, Writing – review & editing, Funding acquisition, Project administration.

#### Data availability

Data associated with the manuscript is available at <https://doi.org/10.23729/8dc295cd-4915-4536-acbc-d0603d54bfb4>.

#### Declaration of Competing Interest

The authors declare the following financial interests/personal relationships which may be considered as potential competing interests: [Maria Sammalkorpi reports financial support was provided by Kemira Oyj. Sousa Javan Nikkhah reports financial support was provided by Kemira Oyj].

#### Acknowledgments

This work was supported by Kemira Oyj, Business Finland Co-Innovation grant No. 3767/31/2019 (M.S.) and the Academy of Finland through its Centres of Excellence Programme (2022–2029, LIBER) under project no. 346111 (M.S.). Useful discussions with Elsi Turunen and Anneli Lepo are gratefully acknowledged. We are grateful for the support by the FinnCERES Materials Bioeconomy Ecosystem and use of the Bioeconomy Infrastructure at Aalto. Computational resources by CSC IT Centre for Science, Finland, and RAMI – RawMatTERS Finland Infrastructure are also gratefully acknowledged.

#### Appendix A. Supplementary material

Supplementary data to this article can be found online at <https://doi.org/10.1016/j.jcis.2022.12.119>.

#### References

- [1] F. Bates, G. Fredrickson, Block copolymer thermodynamics: theory and experiment, *Annu. Rev. Phys. Chem.* 41 (1990) 525–557, <https://doi.org/10.1146/annurev.pc.41.100190.002521>.
- [2] Y. Mai, A. Eisenberg, Self-assembly of block copolymers, *Chem. Soc. Rev.* 41 (2012) 5969–5985, <https://doi.org/10.1039/C2CS35115C>.
- [3] G. Riess, Micellization of block copolymers, *Prog. Polym. Sci.* 28 (2003) 1107–1170, [https://doi.org/10.1016/S0079-6700\(03\)00015-7](https://doi.org/10.1016/S0079-6700(03)00015-7).
- [4] X. Wang, M. Goswami, R. Kumar, B.G. Sumpter, J. Mays, Morphologies of block copolymers composed of charged and neutral blocks, *Soft Matter* 8 (2012) 3036–3052, <https://doi.org/10.1039/C2SM07223H>.
- [5] H. Hu, M. Gopinadhan, C.O. Osuji, Directed self-assembly of block copolymers: a tutorial review of strategies for enabling nanotechnology with soft matter, *Soft Matter* 10 (2014) 3867–3889, <https://doi.org/10.1039/C3SM52607K>.
- [6] M. Müller, Sizing, Shaping and Pharmaceutical Applications of Polyelectrolyte Complex Nanoparticles, in: M. Müller (Ed.), *Polyelectrolyte Complexes in the Dispersed and Solid State II: Application Aspects*, Springer, Berlin, Heidelberg, Germany, 2014; pp. 197–260. [https://doi.org/10.1007/12\\_2012\\_170](https://doi.org/10.1007/12_2012_170).
- [7] J.G. Kennemur, Poly(vinylpyridine) segments in block copolymers: synthesis, self-assembly, and versatility, *Macromolecules* 52 (2019) 1354–1370, <https://doi.org/10.1021/acs.macromol.8b01661>.
- [8] T.N. Hoheisel, K. Hur, U.B. Wiesner, Block copolymer–nanoparticle hybrid self-assembly, *Prog. Polym. Sci.* 40 (2015) 3–32, <https://doi.org/10.1016/j.progpolymsci.2014.10.002>.
- [9] V. Percec, D.A. Wilson, P. Leowanawat, C.J. Wilson, A.D. Hughes, M.S. Kaucher, D.A. Hammer, D.H. Levine, A.J. Kim, F.S. Bates, K.P. Davis, T.P. Lodge, M.L. Klein, R.H. DeVane, E. Aqad, B.M. Rosen, A.O. Argintaru, M.J. Sienkowska, K. Rissanen, S. Nummelin, J. Ropponen, Self-assembly of Janus dendrimers into uniform dendrimersomes and other complex architectures, *Science* 328 (2010) 1009–1014, <https://doi.org/10.1126/science.1185547>.
- [10] H. Tan, C. Yu, Z. Lu, Y. Zhou, D. Yan, A dissipative particle dynamics simulation study on phase diagrams for the self-assembly of amphiphilic hyperbranched multiarm copolymers in various solvents, *Soft Matter* 13 (2017) 6178–6188, <https://doi.org/10.1039/C7SM01170A>.
- [11] H. Kurz, C. Hils, J. Timm, G. Hörner, A. Greiner, R. Marschall, H. Schmalz, B. Weber, Self-assembled fluorescent block copolymer micelles with responsive emission, *Angew. Chem. Int. Ed.* 61 (2022) e202117570.
- [12] S.M. Copp, R.L. Hamblin, K. Swingle, D. Rai, V.S. Urban, S.A. Ivanov, G.A. Montaña, Complex pH-dependent interactions between weak polyelectrolyte block copolymer micelles and molecular fluorophores, *Langmuir* 38 (2022) 2038–2045, <https://doi.org/10.1021/acs.langmuir.1c02889>.
- [13] K. Brassat, J.K.N. Lindner, Nanoscale block copolymer self-assembly and microscale polymer film dewetting: progress in understanding the role of interfacial energies in the formation of hierarchical nanostructures, *Adv. Mater. Interfaces* 7 (2020) 1901565, <https://doi.org/10.1002/admi.201901565>.
- [14] Y. Aviv, E. Altay, O. Burg, M. Müller, J. Rzaev, R. Shenhar, Bottlebrush block copolymer assembly in ultraconfined films: effect of substrate selectivity, *Macromolecules* 54 (2021) 2079–2089, <https://doi.org/10.1021/acs.macromol.0c02057>.
- [15] F. Lv, Z. An, P. Wu, What determines the formation of block copolymer nanotubes?, *Macromolecules* 53 (2020) 367–373, <https://doi.org/10.1021/acs.macromol.9b01868>.
- [16] L.P.D. Ratcliffe, M.J. Derry, A. Ianaro, R. Tuinier, S.P. Armes, A single thermoresponsive diblock copolymer can form spheres, worms or vesicles in aqueous solution, *Angew. Chem. Int. Ed.* 58 (2019) 18964–18970, <https://doi.org/10.1002/anie.201909124>.
- [17] T.I. Löbbling, O. Borisov, J.S. Haataja, O. Ikkala, A.H. Gröschel, A.H.E. Müller, Rational design of ABC triblock terpolymer solution nanostructures with controlled patch morphology, *Nat. Commun.* 7 (2016) 12097, <https://doi.org/10.1038/ncomms12097>.
- [18] R. Nagarajan, M. Barry, E. Ruckenstein, Unusual selectivity in solubilization by block copolymer micelles, *Langmuir* 2 (1986) 210–215, <https://doi.org/10.1021/la00068a017>.
- [19] K. Šindelka, Z. Limpouchová, M. Lísal, K. Procházka, Dissipative particle dynamics study of electrostatic self-assembly in aqueous mixtures of copolymers containing one neutral water-soluble block and one either positively or negatively charged polyelectrolyte block, *Macromolecules* 47 (2014) 6121–6134, <https://doi.org/10.1021/ma501018x>.
- [20] N. Moreno, S.P. Nunes, K.-V. Peinemann, V.M. Calo, Topology and shape control for assemblies of block copolymer blends in solution, *Macromolecules* 48 (2015) 8036–8044, <https://doi.org/10.1021/acs.macromol.5b01891>.
- [21] H. Feng, X. Lu, W. Wang, N.-G. Kang, J.W. Mays, Block copolymers: synthesis, self-assembly, and applications, *Polymers* 9 (2017) 494, <https://doi.org/10.3390/polym9100494>.
- [22] L. Bai, D.J. McClements, Extending emulsion functionality: post-homogenization modification of droplet properties, *Processes* 4 (2016) 17, <https://doi.org/10.3390/pr4020017>.

- [23] P.S. Clegg, J.W. Tavecchi, P.J. Wilde, One-step production of multiple emulsions: microfluidic, polymer-stabilized and particle-stabilized approaches, *Soft Matter* 12 (2016) 998–1008, <https://doi.org/10.1039/C5SM01663K>.
- [24] H. Chen, E. Ruckenstein, Formation of complex colloidal particles: morphologies and mechanisms, *Soft Matter* 8 (2012) 8911–8916, <https://doi.org/10.1039/C2SM26035B>.
- [25] L. Wang, J. Lin, Discovering multicore micelles: insights into the self-assembly of linear ABC terpolymers in midblock-selective solvents, *Soft Matter* 7 (2011) 3383–3391, <https://doi.org/10.1039/C0SM01079K>.
- [26] M. Ueda, A. Hashidzume, T. Sato, Unicore–multicore transition of the micelle formed by an amphiphilic alternating copolymer in aqueous media by changing molecular weight, *Macromolecules* 44 (2011) 2970–2977, <https://doi.org/10.1021/ma102635y>.
- [27] Z. Iatridi, C. Tsitsilianis, pH responsive self assemblies from an  $A_n$ -core-(B-b- $C_n$ ) heteroarm star block terpolymer bearing oppositely charged segments, *Chem. Commun.* 47 (2011) 5560–5562, <https://doi.org/10.1039/c0cc05507g>.
- [28] N. Duxin, F. Liu, H. Vali, A. Eisenberg, Cadmium sulphide quantum dots in morphologically tunable triblock copolymer aggregates, *J. Am. Chem. Soc.* 127 (2005) 10063–10069, <https://doi.org/10.1021/ja0505043>.
- [29] H. Chen, E. Ruckenstein, Formation and degradation of multicomponent multicore micelles: insights from dissipative particle dynamics simulations, *Langmuir* 29 (2013) 5428–5434, <https://doi.org/10.1021/la400033s>.
- [30] C.P. Callaway, S.M. Lee, M. Mallard, B. Clark, S.S. Jang, Effect of block length and side chain length ratios on determining a multicompartment micelle structure, *J. Phys. Chem. B* 123 (2019) 4784–4791, <https://doi.org/10.1021/acs.jpcc.9b02231>.
- [31] Y. Zhao, L.-Y. You, Z.-Y. Lu, C.-C. Sun, Dissipative particle dynamics study on the multicompartment micelles self-assembled from the mixture of diblock copolymer poly(ethyl ethylene)-block-poly(ethylene oxide) and homopolymer poly(propylene oxide) in aqueous solution, *Polymer* 50 (2009) 5333–5340, <https://doi.org/10.1016/j.polymer.2009.09.014>.
- [32] M. Marguet, C. Bonduelle, S. Lecommandoux, Multicompartmentalized polymeric systems: towards biomimetic cellular structure and function, *Chem. Soc. Rev.* 42 (2013) 512–529, <https://doi.org/10.1039/c2cs35312a>.
- [33] A.R. Longstreet, D.T. McQuade, Organic reaction systems: using microcapsules and microreactors to perform chemical synthesis, *Acc. Chem. Res.* 46 (2013) 327–338, <https://doi.org/10.1021/ar300144x>.
- [34] J. Lu, J. Dimroth, M. Weck, Compartmentalization of incompatible catalytic transformations for tandem catalysis, *J. Am. Chem. Soc.* 137 (2015) 12984–12989, <https://doi.org/10.1021/jacs.5b07257>.
- [35] X. Shi, F. Tian, Multiscale modeling and simulation of nano-carriers delivery through biological barriers—a review, *Adv. Theory Simul.* 2 (2019) 1800105, <https://doi.org/10.1002/adts.201800105>.
- [36] F. Cuomo, A. Ceglie, A. De Leonardi, F. Lopez, Polymer capsules for enzymatic catalysis in confined environments, *Catalysts* 9 (2019) 1, <https://doi.org/10.3390/catal9010001>.
- [37] C.T. Womble, M. Kuepfert, M. Weck, Multicompartment polymeric nanoreactors for non-orthogonal cascade catalysis, *Macromol. Rapid Commun.* 40 (2019) 1800580, <https://doi.org/10.1002/marc.201800580>.
- [38] J. Liu, W. Huang, Y. Pang, P. Huang, X. Zhu, Y. Zhou, D. Yan, Molecular self-assembly of a homopolymer: an alternative to fabricate drug-delivery platforms for cancer therapy, *Angew. Chem. Int. Ed.* 50 (2011) 9162–9166, <https://doi.org/10.1002/anie.201102280>.
- [39] M. Naous, D. García-Gómez, F.J. López-Jiménez, F. Bouanani, M.L. Lunar, S. Rubio, Multicore magnetic nanoparticles coated with oligomeric micelles: characterization and potential for the extraction of contaminants over a wide polarity range, *Anal. Chem.* 89 (2017) 1353–1361, <https://doi.org/10.1021/acs.analchem.6b04411>.
- [40] L.S. Grundy, V.E. Lee, N. Li, C. Sosa, W.D. Mulhearn, R. Liu, R.A. Register, A. Nikoubashman, R.K. Prud'homme, A.Z. Panagiotopoulos, R.D. Priestley, Rapid production of internally structured colloids by flash nanoprecipitation of block copolymer blends, *ACS Nano* 12 (2018) 4660–4668, <https://doi.org/10.1021/acsnano.8b01260>.
- [41] A. Nikoubashman, V.E. Lee, C. Sosa, R.K. Prud'homme, R.D. Priestley, A.Z. Panagiotopoulos, Directed assembly of soft colloids through rapid solvent exchange, *ACS Nano* 10 (2016) 1425–1433, <https://doi.org/10.1021/acsnano.5b06890>.
- [42] T.I. Morozova, V.E. Lee, A.Z. Panagiotopoulos, R.K. Prud'homme, R.D. Priestley, A. Nikoubashman, On the stability of polymeric nanoparticles fabricated through rapid solvent mixing, *Langmuir* 35 (2019) 709–717, <https://doi.org/10.1021/acs.langmuir.8b03399>.
- [43] J. Schneider, L.D. Süß, F. Müller-Plathe, The influence of entanglements on the dynamics of flash nanoprecipitation: a slip-spring dissipative-particle-dynamics investigation, *J. Chem. Eng. Data* 65 (2020) 1264–1272, <https://doi.org/10.1021/acs.jced.9b00679>.
- [44] P.-G. De Gennes, Kinetics of collapse for a flexible coil, *J. physique, Lett.* 46 (1985) 639–642, <https://doi.org/10.1051/jphyslet:019850046014063900>.
- [45] T. Chen, A.-P. Hynninen, R.K. Prud'homme, I.G. Kevrekidis, A.Z. Panagiotopoulos, Coarse-grained simulations of rapid assembly kinetics for polystyrene-*b*-poly(ethylene oxide) copolymers in aqueous solutions, *J. Phys. Chem. B* 112 (2008) 16357–16366, <https://doi.org/10.1021/jp805826a>.
- [46] R. Chang, A. Yethiraj, Solvent effects on the collapse dynamics of polymers, *J. Chem. Phys.* 114 (2001) 7688–7699, <https://doi.org/10.1063/1.1361071>.
- [47] N. Li, A. Nikoubashman, A.Z. Panagiotopoulos, Multi-scale simulations of polymeric nanoparticle aggregation during rapid solvent exchange, *J. Chem. Phys.* 149 (2018), <https://doi.org/10.1063/1.5046159> 084904.
- [48] A.L. Harmat, S. Javan Nikkhab, M. Sammalkorpi, Dissipative particle dynamics simulations of H-shaped diblock copolymer self-assembly in solvent, *Polymer* 233 (2021), <https://doi.org/10.1016/j.polymer.2021.124198> 124198.
- [49] S. Javan Nikkhab, E. Turunen, A. Lepo, T. Ala-Nissila, M. Sammalkorpi, Multicore assemblies from three-component linear homo-copolymer systems: a coarse-grained modeling study, *Polymers* 13 (2021) 2193, <https://doi.org/10.3390/polym13132193>.
- [50] Y. Guo, Z. Ma, Z. Ding, R.K.Y. Li, Study of hierarchical microstructures self-assembled by  $\pi$ -shaped ABC block copolymers in dilute solution using self-consistent field theory, *J. Colloid Interface Sci.* 379 (2012) 48–55, <https://doi.org/10.1016/j.jcis.2012.04.056>.
- [51] P.J. Hoogerbrugge, J.M.V.A. Koelman, Simulating microscopic hydrodynamic phenomena with dissipative particle dynamics, *EPL* 19 (1992) 155–160, <https://doi.org/10.1209/0295-5075/19/3/001>.
- [52] P. Espanol, Dissipative Particle Dynamics, in: S. Yip (Ed.), *Handbook of Materials Modeling: Methods*, Springer, Dordrecht, Netherlands, 2005, pp. 2503–2512, [https://doi.org/10.1007/978-1-4020-3286-8\\_131](https://doi.org/10.1007/978-1-4020-3286-8_131).
- [53] R.D. Groot, Electrostatic interactions in dissipative particle dynamics—simulation of polyelectrolytes and anionic surfactants, *J. Chem. Phys.* 118 (2003) 11265–11277, <https://doi.org/10.1063/1.1574800>.
- [54] R.D. Groot, P.B. Warren, Dissipative particle dynamics: Bridging the gap between atomistic and mesoscopic simulation, *J. Chem. Phys.* 107 (1997) 4423–4435, <https://doi.org/10.1063/1.474784>.
- [55] S. Plimpton, Fast parallel algorithms for short-range molecular dynamics, *J. Comput. Phys.* 117 (1995) 1–19, <https://doi.org/10.1006/jcph.1995.1039>.
- [56] A.P. Thompson, H.M. Aktulga, R. Berger, D.S. Bolintineanu, W.M. Brown, P.S. Crozier, P.J. in 't Veld, A. Kohlmeyer, S.G. Moore, T.D. Nguyen, R. Shan, M.J. Stevens, J. Tranchida, C. Trott, S.J. Plimpton, LAMMPS - a flexible simulation tool for particle-based materials modeling at the atomic, meso, and continuum scales, *Comput. Phys. Commun.* 271 (2022), <https://doi.org/10.1016/j.cpc.2021.108171> 108171.
- [57] C. Liu, M.A. Hillmyer, T.P. Lodge, Evolution of multicompartment micelles to mixed corona micelles using solvent mixtures, *Langmuir* 24 (2008) 12001–12009, <https://doi.org/10.1021/la802336k>.
- [58] J. Xia, D. Liu, C. Zhong, Multicompartment micelles and vesicles from  $\pi$ -shaped ABC block copolymers: a dissipative particle dynamics study, *Phys. Chem. Chem. Phys.* 9 (2007) 5267–5273, <https://doi.org/10.1039/B705359B>.
- [59] D. Liu, C. Zhong, Multicompartment micelles formed from star-dendritic triblock copolymers in selective solvents: A dissipative particle dynamics study, *Polymer* 49 (2008) 1407–1413, <https://doi.org/10.1016/j.polymer.2008.01.034>.
- [60] S. Kubowicz, J.-F. Baussard, J.-F. Lutz, A.F. Thünemann, H. von Berlepsch, A. Laschewsky, Multicompartment micelles formed by self-assembly of linear ABC triblock copolymers in aqueous medium, *Angew. Chem. Int. Ed.* 44 (2005) 5262–5265, <https://doi.org/10.1002/anie.200500584>.
- [61] A.F. Thünemann, S. Kubowicz, H. von Berlepsch, H. Möhwald, Two-compartment micellar assemblies obtained via aqueous self-organization of synthetic polymer building blocks, *Langmuir* 22 (2006) 2506–2510, <https://doi.org/10.1021/la0533720>.
- [62] H.v. Berlepsch, C. Böttcher, K. Skrabania, A. Laschewsky, Complex domain architecture of multicompartment micelles from a linear ABC triblock copolymer revealed by cryogenic electron tomography, *Chem. Commun.* (2009) 2290–2292, <https://doi.org/10.1039/B903658J>.
- [63] Z. Li, E. Kesselman, Y. Talmon, M.A. Hillmyer, T.P. Lodge, Multicompartment micelles from ABC miktoarm stars in water, *Science* 306 (2004) 98–101, <https://doi.org/10.1126/science.1103350>.
- [64] R.J.R.W. Peters, M. Marguet, S. Marais, M.W. Fraaije, J.C.M. van Hest, S. Lecommandoux, Cascade reactions in multicompartmentalized polymersomes, *Angew. Chem. Int. Ed.* 53 (2014) 146–150, <https://doi.org/10.1002/anie.201308141>.
- [65] J. Shi, L. Zhang, Z. Jiang, Facile construction of multicompartment multienzyme system through layer-by-layer self-assembly and biomimetic mineralization, *ACS Appl. Mater. Interfaces* 3 (2011) 881–889, <https://doi.org/10.1021/am101241u>.
- [66] M.J. York-Duran, M. Godoy-Gallardo, C. Labay, A.J. Urquhart, T.L. Andresen, L. Hosta-Rigau, Recent advances in compartmentalized synthetic architectures as drug carriers, cell mimics and artificial organelles, *Colloids Surf. B Biointerfaces* 152 (2017) 199–213, <https://doi.org/10.1016/j.colsurfb.2017.01.014>.
- [67] H. Cho, T.C. Lai, K. Tomoda, G.S. Kwon, Polymeric micelles for multi-drug delivery in cancer, *AAPS PharmSciTech* 16 (2014) 10–20, <https://doi.org/10.1208/s12249-014-0251-3>.
- [68] Y. Zheng, H.T. Davis, Mixed micelles of nonionic surfactants and uncharged block copolymers in aqueous solutions: microstructure seen by cryo-TEM, *Langmuir* 16 (2000) 6453–6459, <https://doi.org/10.1021/la000230r>.
- [69] T.S. Banipal, A.K. Sood, Mixed micellar and interfacial interactions of a triblock copolymer (EO<sub>37</sub>PO<sub>56</sub>EO<sub>37</sub>) with a series of monomeric and dimeric surfactants, *J. Surfactant Deterg.* 16 (2013) 881–891, <https://doi.org/10.1007/s11743-013-1516-7>.
- [70] F. Zhao, D. Xie, G. Zhang, S. Pispas, Thermoresponsive complex amphiphilic block copolymer micelles investigated by laser light scattering, *J. Phys. Chem. B* 112 (2008) 6358–6362, <https://doi.org/10.1021/jp800056k>.
- [71] A. Kellarakis, V. Castelletto, M.J. Krysmann, V. Havredaki, K. Viras, I.W. Hamley, Polymer–surfactant vesicular complexes in aqueous medium, *Langmuir* 24 (2008) 3767–3772, <https://doi.org/10.1021/la703745z>.

- [72] M. Jacquin, P. Muller, H. Cottet, R. Crooks, O. Théodoly, Controlling the melting of kinetically frozen poly(butyl acrylate-*b*-acrylic acid) micelles via addition of surfactant, *Langmuir* 23 (2007) 9939–9948, <https://doi.org/10.1021/la700370f>.
- [73] S. Pispas, Soluble complexes of sodium poly(isoprene-*b*-methacrylate) micelles with cationic surfactants in aqueous media, *J. Phys. Chem. B.* 110 (2006) 2649–2655, <https://doi.org/10.1021/jp056008i>.
- [74] M.S. Bakshi, Engineered nanomaterials growth control by monomers and micelles: from surfactants to surface active polymers, *Adv. Colloid Interface Sci.* 256 (2018) 101–110, <https://doi.org/10.1016/j.cis.2018.04.012>.
- [75] A. Abbasi Moud, Rheology and microscopy analysis of polymer–surfactant complexes, *Colloid Polym. Sci.* 300 (2022) 733–762, <https://doi.org/10.1007/s00396-022-04982-2>.